Thermal waveguide OPO

S. T. Lin, Y.Y. Lin, T. D. Wang, and Y.C. Huang*

Institute of Photonics Technologies, Department of Electrical Engineering, National Tsing-hua University, Hsinchu 30013, Taiwan
**ychuang@ee.nthu.edu.tw*

Abstract: We report a mid-infrared, CW singly resonant optical parametric oscillator (OPO) with a thermally induced waveguide in its gain crystal. We measured a numerical aperture of 0.0062 for the waveguide at 80-W intracavity power at 3.2 μm. This thermal-guiding effect benefits to the stable operation of an OPO and improves the parametric conversion efficiency by more than a factor of two when compared with that without thermal guiding.

OCIS codes: (190.4410) Nonlinear optics, parametric processes; (190.4970) Parametric oscillators and amplifiers

References and links

1. S. Schiller, and J. Mlynek, "Continuous-wave optical parametric oscillators, materials, devices, applications," Appl. Phys. B **66**, 664–764 (1998).
2. M. van Herpen, S. Te Lintel Hekkert, S. E. Bisson, and F. J. M. Harren, "Wide single-mode tuning of a 3.0- 3.8-mum, 700-mW, continuous-wave Nd:YAG-pumped optical parametric oscillator based on periodically poled lithium niobate," Opt. Lett. **27**(8), 640–642 (2002).
3. A. K. Y. Ngai, S. T. Persijn, I. D. Lindsay, A. A. Kosterev, P. Groß, C. J. Lee, S. M. Cristescu, F. K. Tittel, K. J. Boller, and F. J. M. Harren, "Continuous wave optical parametric oscillator for quartz-enhanced photoacoustic trace gas sensing," Appl. Phys. B **89**(1), 123–128 (2007).
4. W. R. Bosenberg, A. Drobshoff, J. I. Alexander, L. E. Myers, and R. L. Byer, "Continuous-wave singly resonant optical parametric oscillator based on periodically poled $LiNbO_3$," Opt. Lett. **21**(10), 713–715 (1996).
5. M. Vainio, J. Peltola, S. Persijn, F. J. M. Harren, and L. Halonen, "Singly resonant cw OPO with simple wavelength tuning," Opt. Express **16**(15), 11141–11146 (2008).
6. S. T. Lin, Y. Y. Lin, Y. C. Huang, A. C. Chiang, and J. T. Shy, "Observation of thermal-induced optical guiding and bistability in a mid-IR continuous-wave, singly resonant optical parametric oscillator," Opt. Lett. **33**(20), 2338–2340 (2008).
7. D.W. Chen and T. S. Rose, "Low noise 10-W generation near 3 μm with MgO doped PPLN," Presented at CLEO 2005, CThQ2, Baltimore, USA, 22–27 May 2005.
8. R. O. Moore, G. Biondini, and W. L. Kath, "Self-induced thermal effects and model competition in continuous-wave optical parametric oscillators," J. Opt. Soc. Am. B **19**(4), 802–811 (2002).
9. A. Henderson, and R. Stafford, "Intra-cavity power effects in singly resonant cw OPOs," Appl. Phys. B **85**(2-3), 181–184 (2006).
10. A. Douillet, J. J. Zondy, A. Yelisseyev, S. Lobanov, and L. Isaenko, "Stability and frequency tuning of thermally loaded continuous-wave AgGaS2 optical parametric oscillators," J. Opt. Soc. Am. B **16**(9), 1481–1498 (1999).
11. M. Vainio, J. Peltola, S. Persijn, F. J. M. Harren, and L. Halonen, "Thermal effects in singly resonant continuous-wave optical parametric oscillators," Appl. Phys. B **94**(3), 411–427 (2009).
12. Z. Xiong, Z. G. Li, N. Moore, W. L. Huang, and G. C. Lim, "Detailed investigation of thermal effects in longitudinally diode-pumped Nd:YVO/sub 4/ lasers," IEEE J. Quantum Electron. **39**(8), 979–986 (2003).
13. M. E. Innocenzi, H. T. Yura, C. L. Fincher, and R. A. Fields, "Thermal modeling of continuous-wave end-pumped solid-state lasers," Appl. Phys. Lett. **56**(19), 1831–1833 (1990).
14. B. E. A. Saleh, and M. C. Teich, *Fundamental of Photonics* (John Wiley & Sons, 1991), pp. 54–57.
15. A. E. Siegman, *Lasers* (University Science Books, 1986), pp.786–787.
16. O. Paul, A. Quosig, T. Bauer, M. Nittmann, J. Bartschke, G. Anstett, and J. A. L' Huillier, "Temperature-dependent Sellmeier equation in the MIR for the extraordinary refractive index of 5% MgO doped congruent $LiNbO_3$," Appl. Phys. B **86**(1), 111–115 (2006).

1. Introduction

A wavelength-tunable, narrow-line, continuous-wave (CW), mid-infrared (mid-IR) laser source is useful for spectroscopic applications such as greenhouse gas monitoring and industrial emission control [1–3]. In the past, a 1-μm laser pumped singly resonant optical parametric oscillator (SRO) [4] resonating a near-IR signal wave around 1.5-1.7 μm was often

#120737 - $15.00 USD Received 30 Nov 2009; revised 24 Dec 2009; accepted 24 Dec 2009; published 12 Jan 2010

adopted to generate an idler output at 3-4 μm. A ring-type SRO is capable of generating a single-longitudinal-mode (SLM) output at the resonant wavelength, but the non-resonant wave inherits the linewidth of the pump source [4–6]. Therefore, to generate a single-frequency mid-IR laser, one can use an expensive SLM laser to pump a ring SRO resonating at the near-IR signal wavelength [5] or use an economical multi-longitudinal-mode laser to pump a ring SRO resonating at the idler wavelength [6]. For the latter using MgO:PPLN as its gain medium, slight idler absorption in the crystal could cause thermal lensing and dephasing, which were thought to degrade the performance of an OPO [7–9]. However, the thermal effect in an SRO was also found advantageous in locking the cavity frequency and stabilizing a laser cavity [10,11]. Previously, we have reported thermally induced bistability in a mid-IR single-frequency SRO using an Mg:PPLN gain crystal and showed an unexpected high parametric gain at the high-power state [6]. In this paper, we further provide a theoretical support to the observation and experimentally characterize a thermally induced waveguide in the mid-IR SRO gain crystal.

2. Mid-IR SRO

Figure 1 shows the schematic of the mid-IR SRO. The SRO adopts a bow-tie ring resonator configuration, consisting of two curved mirrors (shown as M_1 and M_2 in the plot) with a 100-mm radius of curvature and two flat mirrors (shown as M_3 and M_4). The four reflecting mirrors are made of IR-grade fused silica to avoid mid-IR absorption in the mirror substrates. All four cavity mirrors have > 99.9% reflectance over a wavelength range from 3200 to 3400 nm, and >97% transmittance from 1550 to 1650 nm and at the pump wavelength. The total cavity length of the ring SRO is 500 mm and the mode radius at the center of the gain crystal is 100 μm. The gain crystal is a 5 mol. % MgO:PPLN crystal (HC Photonics Inc.) with a length of 50 mm and an aperture of 3 mm (*y* direction) × 1 mm (*z* direction). The PPLN crystal has a domain period of 30.7 μm, which was designed to match the phase of the pump, signal, and idler waves at 1.064, 1.59 and 3.2 μm, respectively, at 90°C. The two end surfaces of the MgO:PPLN crystal were optically polished and coated with 0.5, 0.2, and 14% reflectances at the pump, idler, and signal wavelengths, respectively.

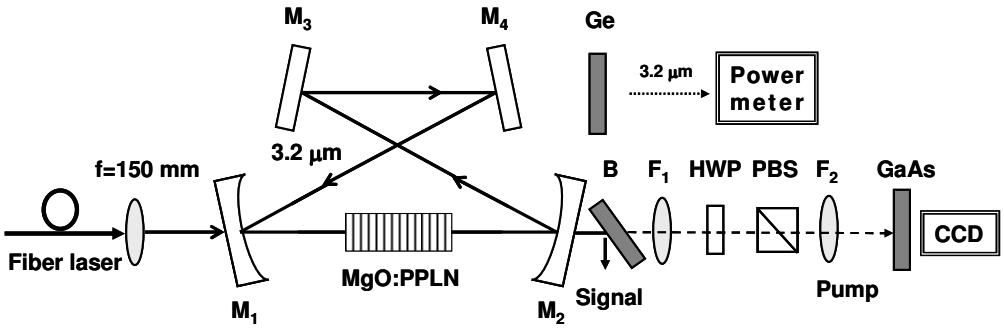

Fig. 1. Experimental setup of the ring mid-IR SRO for characterizing the thermal-induced optical lensing and guiding in the nonlinear crystal, MgO:PPLN. The output pump mode is sensitive to the photothermal effect in the nonlinear crystal. A CCD behind a GaAs filter images the output pump beam as a function of the intracavity idler power to reveal the thermal effects in the SRO. B: a dichroic mirror to kick out the signal wave, HWP: half-wave plate, PBS: polarization beam splitter.

The pump laser we used is a linearly polarized Yb fiber laser (IPG YLM-25-LP) at 1064 nm. The output beam profile of the pump laser is nearly diffraction limited (M^2~1.1) and has a spectral linewidth of 1 nm. The pump beam is polarized along the crystallographic z direction of the MgO:PPLN crystal and is mode-matched into the SRO cavity by using a 150-mm focusing lens.

To characterize the thermal effect in the SRO, we removed the signal wave at the dichroic mirror B and used a set of lenses F_1 and F_2 to image the residual pump beam into a CCD beam

#120737 - $15.00 USD Received 30 Nov 2009; revised 24 Dec 2009; accepted 24 Dec 2009; published 12 Jan 2010

profiler (Ophir-Spiricon LBA-FW-SCOR). An optical attenuator, consisting of a half-wave plate and a polarizer, is sandwiched between the two imaging lenses to optimize the power entering the CCD. A 1 mm-thick, double-side polished GaAs wafer is installed in front of the imaging system to remove the short-wavelength background generated from some non-phase-matched nonlinear optical mixing processes in the crystal. The intracavity idler power is deduced from the idler power exiting mirror M_4. The Ge filter immediately placed after M_4 is used to prevent any residual pump and signal waves from entering the power meter.

Figure 2 is a plot of the intracavity idler power versus pump power, indicating bistability similar to that reported in [6], although the PPLN crystal in this experiment is 2-mm narrower in the width (y) direction compared with that in [6]. As will be shown below, thermal lensing in the PPLN crystal first occurs in the low-power state and thermal guiding dominates in the high-power state. The parametric conversion efficiency is increased by more than a factor of two in the high power state.

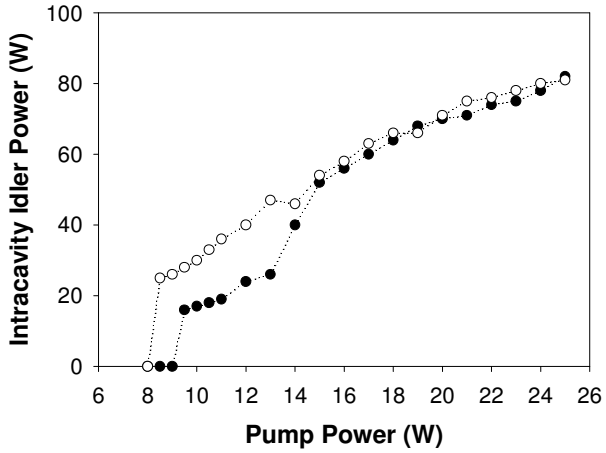

Fig. 2. Intracavity idler power at 3.2 μm versus pump power at 1.064 μm. Thermal lensing in the low power state and thermal guiding in the high power state forms the bistability diagram.

3. Theory of thermal lensing and guiding

Thermal lensing has been studied extensively for solid state lasers [12]. However, unlike a laser, an OPO has several mixing waves in its gain medium. In this section, we derive the thermal focal length and the thermal guiding threshold in a photothermal nonlinear optical material that is slightly absorptive at the idler wavelength and non-absorptive at a probe wavelength. The probe wave can be any of the three mixing waves in an OPO. In the following, the subscript i and p denote the parameters related to the idler and probe waves, respectively.

In general, the refractive index of a photothermal material, n, varies with temperature, characterized by the photothermal coefficient, dn/dT, where T is the temperature variable. Assume an axially symmetric, weakly absorptive MgO:PPLN crystal at the idler wavelength. The idler wave can induce a refractive index change near the axis $r \sim 0$, given by [13]

$$\Delta n_p(r) = -\frac{\alpha_i P_i}{4\pi K}\frac{2r^2}{w_i^2}\frac{dn_p}{dT}, \tag{1}$$

where P_i is the incident idler power, α_i is the absorption coefficient at the idler wavelength λ_i, K is the thermal conductivity of the PPLN crystal, and w_i is the radius of the idler wave. For lithium niobate, K = 5.6W/m/K [8]. The radius w_i in general is a function of the longitudinal

#120737 - $15.00 USD Received 30 Nov 2009; revised 24 Dec 2009; accepted 24 Dec 2009; published 12 Jan 2010

distance z, governed by the expression $w_i(z) = w_{0,i}\sqrt{1+(z/z_{R,i})^2}$, where $z_{R,i} = \pi w_{0,i}^2 n_i / \lambda_i$ is the optical Rayleigh range of the idler wave with $w_{0,i}$ being the waist radius, and n_i being the unperturbed refractive index seen by the idler wave. The additional phase shift for the probe laser, induced by the change of the refractive index, is therefore

$$\Delta\Phi(r) = k_p \Delta n_p(r) \cdot \Delta z, \tag{2}$$

which accounts for the lensing effect through the expression [14]

$$\Delta\Phi(r) = -k_p n_p \frac{r^2}{2} \Delta(\frac{1}{f}), \tag{3}$$

where $k_p = 2\pi/\lambda_p$ is the wave number of the probe laser and f is the thermal focal length. Assume the idler waist coincides with the center of the photothermal material. By substituting (1) into (2), equating (2) and (3), and integrating both side over a total crystal length L, one can obtain the thermal focal length f, given by

$$f = \frac{\lambda_i K}{\alpha_i P_i} \frac{n_p}{n_i (dn_p/dT)} \frac{1}{2\tan^{-1}(L/(2z_{R,i}))}. \tag{4}$$

For the case that the idler waist coincides with the input surface of the material, the term in (4) $2\tan^{-1}(L/(2z_{R,i}))$ is replaced by $\tan^{-1}(L/z_{R,i})$. In the limit of $L/(z_{R,i}) \ll 1$, there is no distinction between these two cases.

The propagation of the complex radius of curvature of a Gaussian laser beam q through a infinitesimal thin lens obeys the rule $1/q_2 = 1/q_1 - 1/f$ [15], where $q_{1,2}$ are the input and output complex radii of curvature of the Gaussian beam, respectively. For a differential change Δq over a differential distance Δz in a photothermal material, one has $\Delta q = q^2 \Delta(1/f)$ or

$$\frac{\Delta q}{\Delta z} = q^2 \frac{\alpha_i P_i}{\pi n_p K w_i^2} \frac{dn_p}{dT}. \tag{5}$$

For a free propagating Gaussian beam, the propagation of the complex radius of curvature is defined as $q = z + jz_R$. Therefore, $dq/dz = 1, 0$ for a diffraction beam and a non-diffraction beam, respectively. Taking into account the diffraction of a Gaussian laser beam in free space, Eq. (5) is modified to be

$$\frac{\Delta q}{\Delta z} = q^2 \frac{\alpha_i P_i}{\pi n_p K w_i^2} \frac{dn_p}{dT} + 1. \tag{6}$$

Equation (6) can also be obtained by directly writing $\Delta q = q^2 \Delta(1/f) + \Delta z$, which is the change of the complex radius of curvature of a Gaussian beam propagating through a thin lens with a differential length Δz. Thermal guiding occurs when the diffraction is exactly offset by thermal focusing. By setting $\Delta q/\Delta z = 0$ in (6), one can determine the critical idler power at the onset of thermal guiding. For example, suppose a probe wave is incident on a photothermal material with its waist coinciding with an idler waist on the front surface of the material. Substituting $q = jz_{R,p} = jn_p \pi w_{0p}^2 / \lambda_p$ into (6) to obtain the critical idler power for guiding the probe laser

$$P_{cr} = \frac{\lambda_p K}{\alpha_i z_{R,p}} \left(\frac{w_{0,i}}{w_{0,p}}\right)^2 \frac{1}{dn_p/dT}. \tag{7}$$

The critical idler power is higher for a longer probe laser wavelength or a shorter probe-laser Rayleigh range, because a longer wavelength or a short Rayleigh range gives faster diffraction. The critical power is reduced for large idler absorption or a large α_i. It is also reasonable that the critical power is proportional to the heat conductivity and inversely

#120737 - $15.00 USD Received 30 Nov 2009; revised 24 Dec 2009; accepted 24 Dec 2009; published 12 Jan 2010

proportional to the photothermal coefficient of the material. In our experiment, we measured α_i = 0.49%/cm at λ_i = 3.2 μm in the Mg-doped PPLN crystal. When the probe laser is the idler wave itself, the critical idler power for self guiding is 47 W for $dn_i/dT = 3.75 \times 10^{-5}$/K [16], w_{0i} = 100 μm, and n_i = 2.08 [16]. This idler power is about the value for the SRO to fully reach the high-power state in Fig. 2. However, according to Eq. (7), thermal guiding for the pump and signal waves can occur earlier than that for the idler wave, which explains the fairly noticeable increase of the parametric efficiency when the intracavity idler power is increased from 20 to 50 W.

4. Experimental characterization of thermal lensing and guiding

Figure 3 shows the recorded pump-beam profiles versus the intracavity idler power in the low-power state. We first inserted a beam stop between M_3 and M_4 and recorded the output pump-beam profile without parametric oscillation. We then removed the beam stop, started the SRO oscillation, and recorded the variation of the pump-beam profile in the CCD versus the intracavity idler power. In the low power state, we found that the pump-beam profile at the output of mirror M_2 was expanded as the intracavity idler power was increased. Owing to the slab structure of the PPLN crystal, the expanded pump-beam profile shows asymmetric thermal lensing along the two transverse directions. When the intracavity power reached 28 W, the beam radius in the z direction is twice that of the cold cavity. However, the beam expansion in the y direction is less obvious. The thin crystal dimension along z gives a larger temperature gradient and thus stronger focusing in that direction.

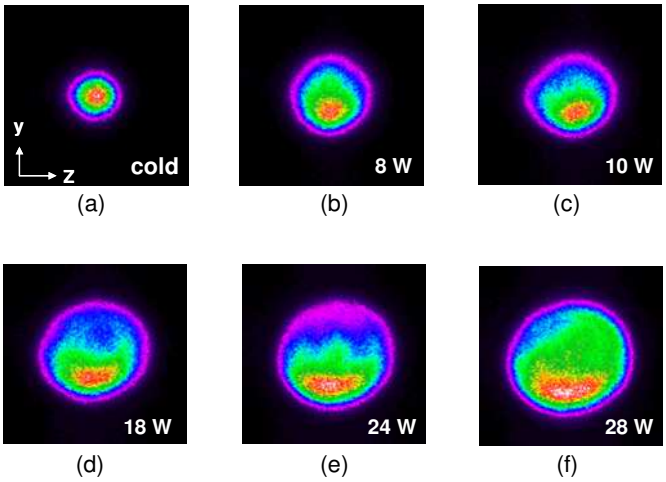

Fig. 3. Output pump-beam profiles at different intracavity idler powers. In (a), the SRO was not in operation. From (b) to (f), the SRO was in the low power state, and the intracavity idler power varied from 8 to 28 W. The images show asymmetric thermal lensing in the two transverse directions.

We used a thin-lens model [10,11] to plot the focal length of the thermal lens as a function of the intracavity idler power in Fig. 4. The focal length in the z direction is a factor of two shorter than that in the y. For comparison, we plot Eq. (4) in the same figure. It is shown that the theoretical curve can reasonably explain the experimental data on the right half of the figure but departs from the experimental data at low idler powers. When the idler power is low, heating of the crystal from both the signal and pump waves could be significant or comparable to that from the idler wave. This would allow the theoretical curve to approach the experimental data at low idler powers.

#120737 - $15.00 USD Received 30 Nov 2009; revised 24 Dec 2009; accepted 24 Dec 2009; published 12 Jan 2010

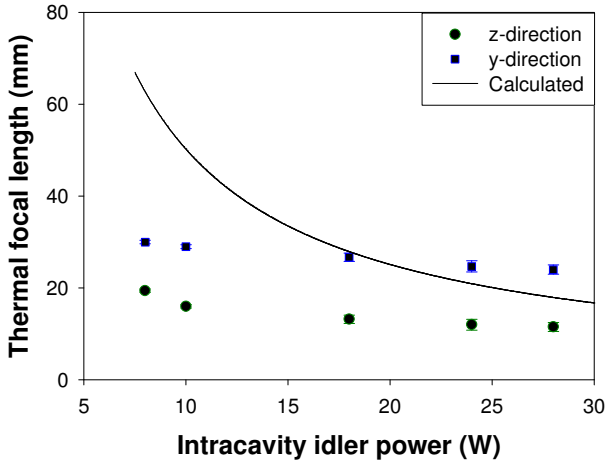

Fig. 4. The focal length of the thermal lens versus intracavity idler power along the thickness (z) and width (y) directions of the crystal. The theoretical curve calculated from Eq. (4) fits better to the experimental data on the right half of the figure. At a low idler power, heating of the crystal by the signal and pump waves might not be ignored.

As soon as the mixing waves are guided in the PPLN crystal, the sudden increase of the intracavity idler power provides fast heating to the MgO:PPLN crystal. As a result, we found that it took a few minutes for our PID temperature controller to stabilize the crystal temperate back to the phase matching temperature in the steep slope regime between the two power states in Fig. 2. Thermal lensing can induce both longitudinal and transverse temperature gradients in the PPLN crystal. The longitudinal temperature gradient could cause phase mismatch to the mixing waves and limit the parametric gain for the OPO. However, there is no longitudinal temperature gradient in a longitudinally uniform thermal waveguide. For our case, the thermal guiding effectively removes the potentially devastating longitudinal temperature gradient in the nonlinear crystal.

As can be seen from Fig. 5, the waveguide confinement to the pump beam and also to all the mixing waves becomes stronger, when the intracavity idler power grows larger. It is interesting to see the spatial shift of the pump beam center when the bistability state is switched from one to the other. The pump-beam displacement is due to the non-ideal alignment of the pump beam to the idler mode in the SRO. This pump-beam pulling phenomenon allows nearly perfect mode overlapping for all mixing waves as soon as the thermal guiding takes place. Once the thermal waveguide is formed in the crystal, the SRO becomes highly efficient and is relatively insensitive to the adjustment of the cavity mirrors.

To measure the numerical aperture (NA) of the thermal waveguide, we carefully tuned the angle of the M_1 mirror so as to move the thermal waveguide relative to the pump-beam angle until the pump beam was switched from a guiding to a lensing mode. Since oscillation of the SRO was maintained during our measurement, we assume that the slight adjustment on the angle of mirror M_1 does not vary the cavity mode significantly. Table 1 summarizes the measured NA values at four pump powers and the corresponding intracavity idler powers. As expected, the NA increases with the pump or the intracavity idler power. The NA value can be considered as the tolerance to the pump-laser or resonator alignment. Once the thermal waveguide was formed and the OPO operated in the high-power state, the OPO became very insensitive to misalignment and vibration. The thermal waveguide greatly improves the SRO stability and increases the tolerance to alignment.

#120737 - $15.00 USD Received 30 Nov 2009; revised 24 Dec 2009; accepted 24 Dec 2009; published 12 Jan 2010

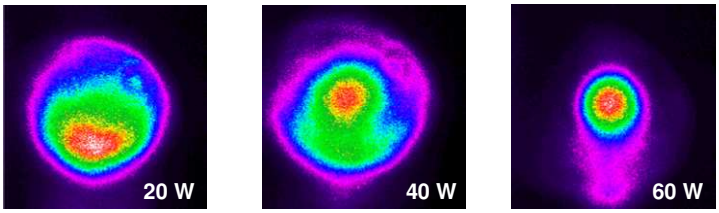

Fig. 5. Pump beam profiles at the SRO output at 20-, 40-, and 60-W intracavity idler powers. At 60 W, the pump wave is tightly guided in the PPLN. During the formation of the thermal waveguide, an imperfectly aligned pump beam can be gradually pulled into the waveguide.

Table 1. Measured numerical aperture of the thermal waveguide versus pump power of the SRO. The corresponding intracavity idler power is also listed. As expected, the NA increases with the pump and intracavity idler powers. The NA provides a reference to the tolerance of the pump-laser and cavity alignment.

Pump power (W)	Intracavity idler power (W)	NA
12	36	0.0017
15	56	0.0039
20	64	0.0054
25	80	0.0062

5. Conclusion

In conclusion, we have analyzed and characterized the thermal lensing and guiding in a mid-IR SRO. We derived a theory to calculate the thermal focal length and estimate the threshold guiding power in a photothermal nonlinear optical material. Unlike the thermal effects in a solid-state laser, those in an OPO are coupled through several mixing waves. In our SRO, the thermal lensing occurs first and thermal guiding follows, when the pump or intracavity idler power is increased. We show in the experiment the pulling and trapping of the pump beam into the thermal waveguide during the formation of the waveguide. For the first time, the numerical aperture of a thermal waveguide in an OPO is measured to show gradual formation of the waveguide when the intracavity idler power is increased. The numerical aperture can be considered as the tolerance to the pump-laser or resonator alignment for such an SRO.

Thermal guiding has a much more profound effect in an OPO than a laser, because, due to the nonlinear mixing process, an OPO is more sensitive to the intensity of a mixing wave. A thermal waveguide helps confine one or several of the mixing waves and increase their intensities for nonlinear frequency conversion. As a result, the parametric efficiency was increased twice in our SRO when the thermal-guiding threshold was reached. Once the thermal waveguide is formed in the nonlinear crystal, the SRO is fairly insensitive to the misalignment of the pump beam or the cavity mirrors.

Acknowledgments

The work is supported by National Defense Industrial Development Foundation under NTHU Project Code 98A0030N6 and by National Science Council under Contract NSC 98-2622-M-007-001-CC1.

#120737 - $15.00 USD Received 30 Nov 2009; revised 24 Dec 2009; accepted 24 Dec 2009; published 12 Jan 2010